Weldability of ductile cast iron using AISI-316L stainless steel ER rod

Javier Cárcel Carrasco, Fidel Salas Vicente*, Aurora Martínez Corral, Manuel Pascual Guillamón

Instituto de Tecnología de Materiales, Universitat Politècnica de València, Camino de Vera, s/n. 46066. Valencia, Spain

(*Corresponding author: fisavi@dimm.upv.es)

ABSTRACT: This paper analyzes the corrosion resistance and the mechanical and microstructural properties of a welded joint of ductile cast iron using AISI316L stainless steel as filler material and three different heat treatments: preheating at 250 and 450 ºC and a post-weld annealing treatment. The results show the presence of ledeburite at the interface between the weld bead and the heat affected zone and at the root pass, along with a loss of strength and ductility when the welding coupons are preheated. An annealing does not eliminate the presence of ledeburite and leads to a massive precipitation of chromium carbides at the areas of the weld bead where dilution is higher. Corrosion rate was lower for the annealed coupon, but in that case, the corrosion of the weld bead increases due to the precipitation of chromium carbides.

KEYWORDS: AISI-316L; Annealing; Cast iron; Corrosion; Preheat; Weldability

RESUMEN: *Soldabilidad de la fundición dúctil usando aporte de acero inoxidable.* Este trabajo analiza la resistencia a la corrosión y las propiedades mecánicas y microestructurales de una unión soldada de fundición dúctil cuando se usa acero inoxidable AISI-316L como material de aporte y tres tratamientos térmicos distintos: precalentamiento a 250 y 450 ºC y un recocido post-soldeo. Los resultados muestran presencia de ledeburita en la interfase y entre la soldadura y la zona afectada por el calor y en la pasada de raíz, además de una pérdida de ductilidad cuando los cupones de soldadura se precalientan. Un recocido no elimina la presencia de ledeburita y lleva a una precipitación masiva de carburos en las zonas de la soldadura donde la dilución es mayor. La velocidad de corrosión fue menor en la unión recocida, pero en ese caso, la corrosión del cordón aumentó debido a la precipitación de carburos de cromo.

PALABRAS CLAVE: AISI-316L; Corrosión; Hierro fundido; Precalentar; Recocido; Soldabilidad

ORCID ID: Javier Cárcel Carrasco (https://orcid.org/0000-0003-2776-533X); Fidel Salas Vicente (https://orcid.org/0000-0003-0834-4425); Aurora Martínez Corral (https://orcid.org/0000-0001-8222-0864); Manuel Pascual Guillamón (https://orcid.org/0000-0003-0216-5119)

1. INTRODUCTION

Ductile cast iron, also known as spheroidal graphite cast iron or nodular cast iron, is an alloy of iron with carbon in an amount that ranges from 3 to 4%. This carbon appears as nodules due to the presence of magnesium in the ladle during casting in percentages between 0.03 and 0.04%. The spheroidal shape of graphite provides this type of cast iron good mechanical properties and corrosion resistance, so that it can often replace steel (Soffritti *et al.*, 2020) and other materials such as aluminium or bronze for wear-resistant applications (Akdogan and Stolarski, 2003). Furthermore, the casting of ductile cast irons provides one of the best ways to obtain components of complex geometry, even when their size (Suárez-Sanabria and Fernández-Carrasquilla, 2006) or the acting loads the part support seem an obstacle (Čanžar *et al.*, 2012). Consequently, it is used for the manufacturing of valves and hydraulic pump housings as well as for drinking water or sewage line pipes (Makar, 2000). In this last case, one of the advantages of ductile cast iron is its mechanical strength, which means it does not require an additional mechanical protection like plastics which are much lighter than metals but due to their low hardness and stiffness sometimes require protection to prevent physical damage. Regarding its structural characteristics, it is worth mentioning that the tensile strength of ductile iron ranges from 480 MPa to 930 MPa, with a modulus of elasticity higher than that of grey cast iron, in the order of 170 GPa. Nevertheless, it maintains the low weldability of all cast irons when compared to other iron alloys (El-Banna, 1999).

Although the welding of ductile cast iron is uncommon in the industry, sometimes it is necessary to join different parts or to repair cracked or fractured elements. These types of joints have been studied using SMAW (Shielded Metal Arc Welding), MIG-MAG (Metal Inert Gas - Metal Active Gas) and TIG (Gas Tungsten Arc Welding) procedures, along with the use of different filler materials such as 97% or 57% Ni-Fe rods (Pouranvari, 2010; Cárcel-Carrasco *et al.*, 2016; Chamim *et al.*, 2017). The advantage of these materials, the most used ones when welding cast iron, is based on obtaining mechanical characteristics for the joints similar to those of the base material. The disadvantage is the increase of price of these joints due to the high price of Ni. Thus, the current research is aimed at evaluating the use of alternative and cheaper filler materials, such an austenitic stainless steel, with a lower Ni content but still capable of avoiding a martensitic transformation of the weld bead during a fast cooling. An evaluation of the corrosion resistance, which is another important feature that welded joints must have in some circumstances, has been included (Zhou *et al.*, 2007; You *et al.*, 2020).

2. MATERIALS AND METHODS

2.1. Materials

The base material used in this paper was a nodular ferritic-perlitic cast iron with a percentage of pearlite of approximately 40%. In this type of casting graphite appears in a nodular shape surrounded by ferrite (Fig. 1), avoiding the graphite sheets that appear in lamellar grey cast iron and act as discontinuities that generate large stress concentrators, reducing the mechanical properties of the alloy.
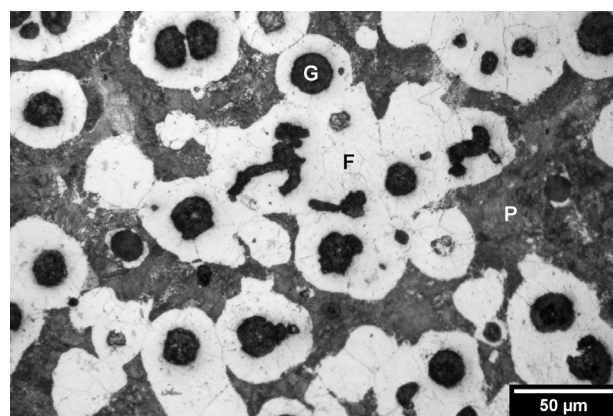

Figure 1. Microstructure of the nodular cast iron used in the study. P: Perlite; G: Graphite; F: Ferrite

The filler material was an AISI 316L stainless steel ER rod, whose main alloy elements are Cr and Ni, but also contains Mn and Mo. Mo improves its corrosion resistance. Its low carbon content serves to prevent the formation of chromium carbide during regular welding practices. This material, which has very good corrosion resistance, is widely used in the food, chemical and petrochemical industries.

Table 1 shows the chemical compositions of both materials and their mechanical characteristics. The mechanical properties of the cast iron where obtained at our laboratory.

2.2. Coupons and welding processes

In order to execute the tests to determine the microstructural, resistant and corrosive characteristics of the welds, it was necessary to obtain a series of test pieces from three coupons. Each one has consisted of two sheets of 250x50x6 mm thick, to which a 30° angle chamfer had been made on each of them on the side of the 50 mm width so that the angle formed at the joint was 60 °C. The welds were carried out using the TIG welding procedure, which was executed with the following parameters: 130 Amperes, 20 Volts and an Argon gas flow of 11 litres per minute, being the first

TABLE 1. Chemical composition (wt.-%) and properties of the nodular cast iron and the AISI 316L steel rod

Chemical composition									
Material	C	Si	Mn	Cr	P	S	Ni	Mo	Mg
AISI 316L	<0.025	0.4	1.5	19	0.03	0.015	12	3	-
Ductile cast iron	3.5	2.9	0.25	-	0.03	0.03	-	-	0.05
Mechanical properties									
				AISI 316L			Nodular cast iron		
Tensile strength (MPa)				530-680			420		
Yield strength (MPa)				240			340		
Total elongation (%)				40			14		
Young modulus (GPa)				190			300		

required step to fix the sheets through light tack welding. The welding process was different for each coupon, however, in every case, at the end of the welding the weld was covered with a ceramic blanket in order to reduce the cooling speed.

The first coupon was introduced, once tack welded, in an oven at 250 ºC, keeping it at this temperature for 30 min to then remove it and proceed to perform the root welding, using 40 mm long sections to avoid deformations and cracking due to residual stresses. Once the root welding had been carried out, the filler welding was executed with precaution of hitting the sections of the weld bead in order to minimize the stresses generated during the welding process until the whole joint was completed. The welding of the second coupon was carried out in the same way than the previous one, but preheating it at 450 ºC.

The third weld coupon was preheated, just as the first one, to 250 ºC, but an annealing post-weld heat treatment was carried out at 900 ºC during one hour, leaving the sample to cool inside the furnace.

Once obtained all three, the necessary test pieces were cut from each coupon to evaluate the mechanical strength characteristics and their resistance to corrosion and to study their microstructure. So, six 20 mm wide test pieces for tensile tests, three test pieces for corrosion tests and a metallographic sample were obtained from each coupon.

2.3. Testing methods

Tensile tests were carried out in a universal testing machine Ibertest Electrotest-100-MD2 of 100 kN following the indications of the UNE-EN ISO-6892-1 standard at a speed of 5 mm×min^{-1}.

The hardness values of the samples were determined using a Vickers microhardness tester, model INNOVA TEST 400A SERIES, with a load of 300 g and a dwell time of 10 s. Two line hardness measurements were taken on each sample, covering the base metal, the heat affected zone, the fusion line, and the weld bead, although additional measurements were taken for the root pass and to characterize the mean hard-

ness of each zone (5 extra measurements per zone). The indications of the UNE-EN ISO 643 standard were followed. To determine the corrosion resistance of the welded samples, they were immersed for 72 h in a 15% ferric chloride salt solution (FeCl3-15%). The samples were weighted before and after the corrosion test using a KERN 770 precision balance.

Finally, the metallographic samples were embedded in methacrylate and grinded using 220 and 500 grit abrasive paper and polished using 3- and 1-µm diamond paste. Lastly, the samples were etched with Nital-3% and using an electrolytic etching bath with 10% oxalic acid in order to reveal the microstructure of the weld bead.

3. RESULTS AND DISCUSSION

3.1. Microstructure

The microstructures at the different zones of the joint obtained for the sample of nodular cast iron preheated to 250 ºC and cooled coating it with a ceramic material can be observed in Fig. 2.

The four micrographs of Fig. 2 show four different zones. At the heat affected zone (Fig. 2a) the microstructure ranges from a ferritic-pearlitic structure with well-defined graphite nodules surrounded by a ferrite crown to a harder structure nearer the fusion line were coarse perlite is progressively replaced by fine perlite and bainite. The changes also seem to include a decrease in the size of the area of ferrite surrounding the graphite nodules.

Figure 2b shows the microstructure at the interface zone. That zone is characterized by the presence of hard cementite in acicular shape. Other hard and brittle microconstituents are also present: a certain proportion of ledeburite and bainite or fine perlite in the darker grains. This microstructure gives the zone the highest hardness of all the union. Regarding the nodules of graphite, they are smaller and have more irregular shape than those of the ductile cast iron nodules.

The microstructure of the weld bead at the filling pass (Figs. 2c and 2d) is different from the microstruc-
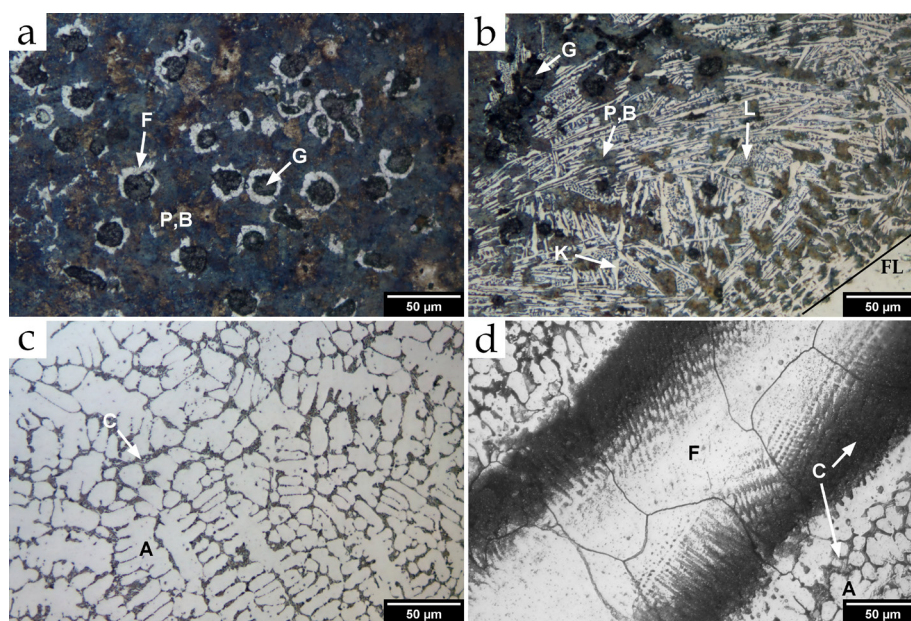
FIGURE 2. Micrographs of the coupon preheated at 250 ºC; a) HAZ, b) Interface, c) Filling pass, d) Ferrite surrounded by carbides in an austenitic matrix at the root pass. P: Perlite; G: Graphite; F: Ferrite; B: Bainite; K: Cementite; L: Ledeburite; A: Austenite; C: Chromium carbides; FL: Fusion line

ture at the root pass due to the higher dilution at the root pass (over 40%). The microstructure of the filling pass consists of an austenitic matrix with the presence of chromium carbides precipitates at the interdendritic space. These precipitates give the matrix a significant increment in hardness with respect to the cast iron or the AISI-316 rod.

The root pass presents a different microstructure. Although a great part of the root pass is also composed of an austenitic matrix, both the higher dilution (higher carbon content) and the heat supplied by the filling pass have led to a larger quantity of carbides in the matrix. Furthermore, the homogeneity of the root pass is far from perfect and some regions of ferrite (not mixed with the filling metal) are surrounded by a huge quantity of chromium carbides (Fig. 2d), or areas with cementite and bainite or tempered martensite can be found (Fig. 3d). These last areas resemble the microstructure of a white cast iron alloy (Vander Voort, 2005).

The four micrographs from Fig. 3 show the microstructures of the union that has been previously preheated at 450 ºC and has not received an additional heat treatment after welding.

The microstructures are very similar to Fig. 2 although as the cooling rate was lower some differences can be mentioned. The crowns surrounding the graphite nodules at the HAZ near the interface are bigger (Fig. 3a) and the amount of perlite/bainite at the interface are also higher (Fig. 3b), with a measured hardness a bit higher in this case. The aspect of the weld bead is very similar to that of the sample preheated at 250 ºC, mainly austenitic, but with a lack of homoge-

neity and the presence of undissolved ferrite and areas resembling the microstructure of a white cast iron alloy (Fig. 2d and 3d).

Figure 4 shows the micrographs of the weld when the coupon has been previously preheated to 250 ºC and has been subjected to annealing heat treatment at 900 ºC with cooling inside the furnace.

As it can be seen in Fig. 4a, the microstructure of the HAZ shows that the matrix has an almost totally ferritic structure with evenly distributed graphite nodules due to the migration of the carbon contained in the pearlite to the graphite nodules.

At the interface zone (Fig. 4b), the presence of ledeburite is still visible despite the annealing, what maintains the hardness of the zone over 700 HV. The matrix at that zone is now pearlitic, just as at the nearer area of the HAZ, that now is reduced to a width of around 200 μm.

Apart from the ferritization of the base metal, the most important changes take place at the weld bead. Figure 5c shows a larger presence of chromium carbides at the filling pass than Figs. 2c or 3c, mainly inside the dendritic grains due to the reaction of the dissolved carbon with the chrome of the AISI-316L steel at 900 ºC (Moustafa *et al.*, 2000). Surprisingly, this does not translate into a notable increment of the weld bead hardness after the annealing. Something similar happens at the root pass, where the dilution is really high and, so, also the presence of free carbon. This leads to the precipitation of a high quantity of carbides, both cementite and chromium carbides, remaining mostly unchanged the white cast iron areas. Figure 5d shows two different zones of the root pass.
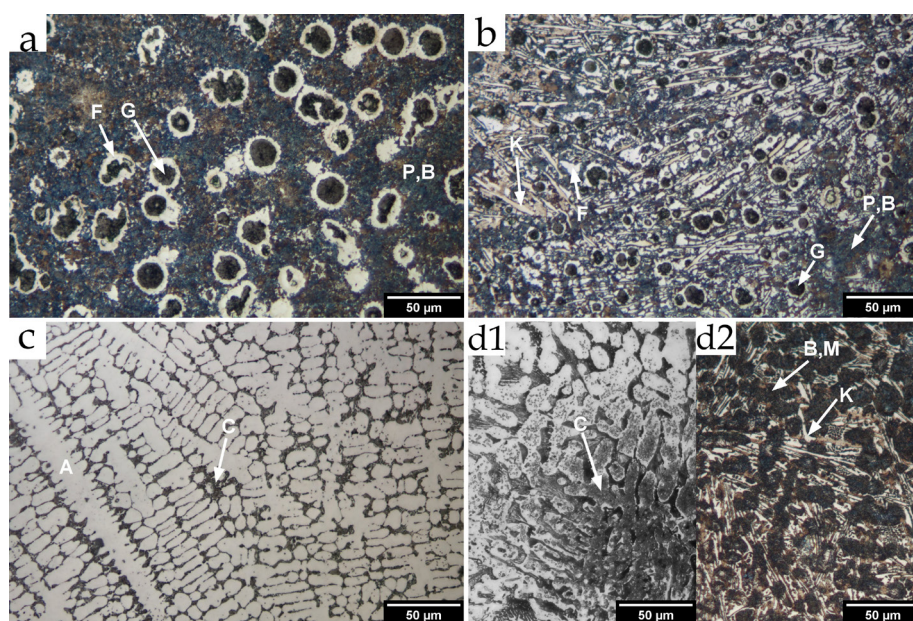
FIGURE 3. Micrographs of the coupon preheated at 450 ºC; a) HAZ, b) Interface, c) Filling pass, d1) High concentration of chromium carbides in an austenitic matrix at the root pass; d2) Area of the root pass with a microstructure similar to a white cast iron. P: Perlite; G: Graphite; F: Ferrite; B: Bainite; M: Martensite; K: Cementite; A: Austenite; C: Chromium carbides.
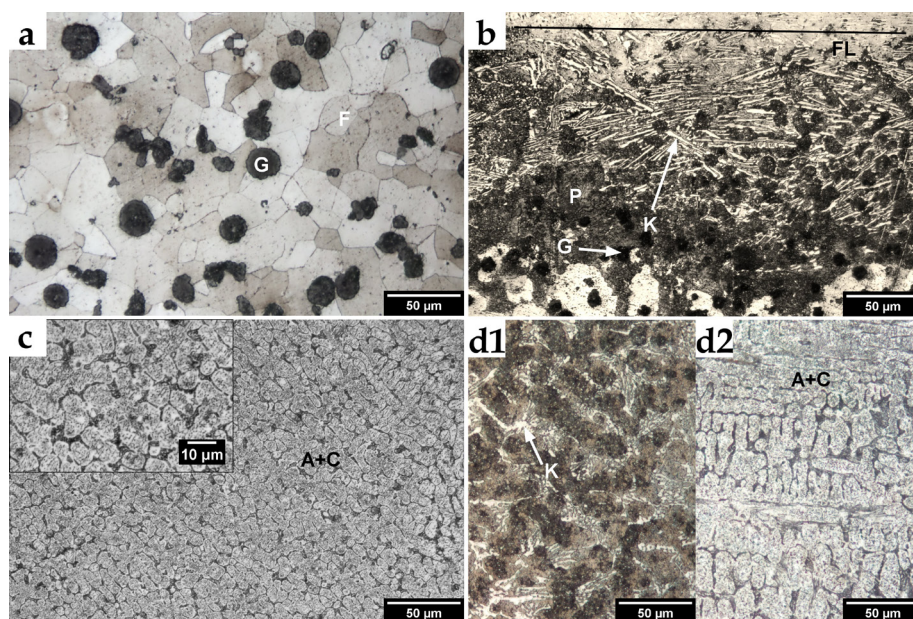

FIGURE 4. Micrographs of the coupon preheated at 250 ºC and annealed at 900 ºC; a) HAZ, b) Interface, c) Filling pass, d1) Area of the root pass with a microstructure similar to a white cast iron; d2) Carbides in an austenitic matrix. G: Graphite; F: Ferrite; B: Bainite; K: Cementite; P: Perlite; A+C: Chromium carbides in austenite; FL: Fusion line.

3.2. Hardness

The values of the properties obtained in the tensile and hardness tests can be observed in Table 2. These values correspond to the average values of each set of test pieces. Figure 5 shows the hardness profile at the joint for the different welding processes.

The hardness profile is very similar for both pre-heated samples without post-weld heat treatment, with a hardness peak at the interface between the weld bead and the heat affected zone (HAZ) around 750 HV and a hardness at the weld bead between 380 and 450 HV. The hardness drops drastically after annealing at the heat affected zone (HAZ), but maintains similar values
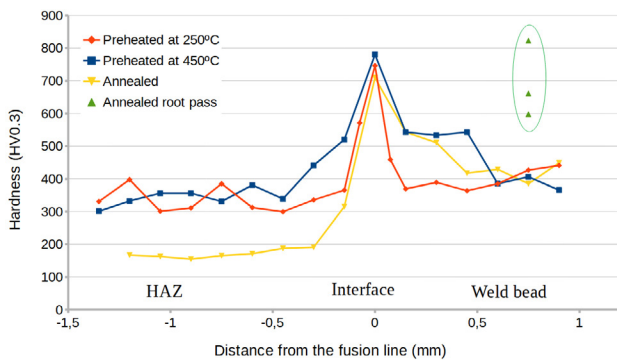
FIGURE 5. Evolution of the mean hardness at the joint. The 0 value on the X-axis corresponds to the fusion line and the positive values corresponds to the weld bead. Green triangles indicate values measured at the white iron cast-like areas of the root pass.

at the interface due to the fact that the hard cementite present in that zone was not dissolved by the annealing (it is still visible at Fig. 5 showing a needle shape).

Regarding the weld bead, the filler material does not contain enough carbon for the carbides to form, but as part of the base material is melted and mixed with the filler material, the carbon content of the weld bead increases notably, leading to the precipitation of chromium carbides. Hardness at the filling passes of the weld bead increases a mean of 200 HV units with respect to the hardness of a typical 316L steel, but at the root pass, where dilution is higher and the carbon content is, hence, also higher, hardness reaches values that range from 600 HV to over 800 HV at the areas where a great concentration of carbides or the presence of cementite is visible. This problem is worse for the annealed sample due to a larger precipitation of hard carbides during the annealing at 900 ºC (Moustafa *et al.*, 2000; Bedolla-Jacuinde *et al.*, 2003), although higher temperatures could lead to their dissolution (Gadhikar *et al.*, 2011). The aspect of the microstructure at the annealed root pass can be seen in Fig. 4.

3.3. Mechanical strength

Regarding the mechanical strength of the different joints when compared to those of the nodular

cast iron (Table 1), the samples preheated at 250 and 450 ºC show very similar strength values, with a mean decrease for the ultimate strength (σ_R) of 7.5% and a mean increment in the yield strength (σ_Y) of 8.8%. The different behavior of the ultimate and the yield strength is a proof of the more brittle behavior of the joint when compared to the base material. In fact, the elongation drops from 14% to 8% and 7%, what reveals, along with the study of the microstructure, there is little between preheating at 250 or 450 ºC.

When the sample preheated at 250 ºC is annealed at 900 ºC the mechanical strength is reduced notably. The ultimate strength is now 62.6% and the yield strength 73.5% of the values corresponding to the base material. This decrease is also accompanied by an increment in elongation, that now reaches 9.5%, but still clearly lower than that of the cast iron. This fact is also anticipated by the fact that the values σ_R and σ_Y are also very close in this case ($\sigma_Y/\sigma_R = 0.95$).

The higher presence of carbides at the weld bead of the annealed weld induced a change in the way the weld breaks during the tensile tests. The fracture of the test pieces with preheating treatment at 250 ºC or 450 ºC took place at the interface (one of the samples preheated at 450 ºC broke at the weld bead), but when the joint was annealed the fracture took place preferably at the middle of the weld bead, showing a change in behavior. This shows that the zone where the breakage takes places coincides with the zone where the hardness is maximum and, thus, ductility is expected to be the lowest.

3.4. Corrosion

Regarding the corrosion resistance of the welded joint, Table 3 shows the mass loss observed for each of the coupons tested. As it is shown in this table, the best corrosion resistance is associated with the annealed microstructure, which is the closest to the thermodynamic equilibrium, being the most susceptible coupon to corrosion the one preheated at 250 ºC (where a microstructure of higher hardness was obtained), with a percentage of material loss twice that of the annealed sample.

TABLE 2. Strength and hardness of the joint according to the heat treatment applied

	Yield strength	Ultimate strength	Total elongation	HV		
	(MPa)	(MPa)	(%)	HAZ	Fusion line	Weld bead
Preheated to 250 ºC	360±12	387±19	7±1	520±25	746±27	405±37
Preheated to 450 ºC	380±14	395±10	8±1	571±20	780±30	386±35
Annealed at 900 ºC	250±21	263±19	9.5±2	315±12	709±24	420±52
All samples						>600*

*At the root pass for the white cast iron areas.

TABLE 3. Mass loss due to corrosion

	Mean initial mass of samples (g)	Mean final mass of samples (g)	Average mass loss (%)
Preheated at 250 ºC	39.64±0.02	37.70±0.02	4.89
Preheated at 450 ºC	38.43±0.03	37.15±0.04	3.32
Preheated at 250 ºC and annealed	37.35±0.01	36.56±0.04	2.10

The mass loss due to corrosion was important at the zones of the weld bead where precipitation of chromium carbides occurred due to having a larger zone of mixing between the filler metal and the base metal (near the interface for the non-annealed samples and the root pass for the annealed sample). The presence of these carbides decreases the amount of protective chromium that is present in solid solution, causing the corrosion resistance to be lower than that of cast iron.

4. CONCLUSIONS

From the testing carried out on the welds made with different treatments, the following conclusions can be outlined:

− No matter the preheating temperature (250 or 450 ºC), the presence of ledeburite at the interface gave that zone a hardness over 700 HV. This results in an ultimate strength close to the base metal but also in a loss of ductility which can reach up to 50%.

− Areas with a high concentration of chromium carbides and with the microstructure of a white cast iron are present at the root pass due to the high dilution rates and lack of homogeneity. These areas show very high harness levels.

− An annealing at 900 ºC ferritizes the matrix of the cast iron, but it is unable to reduce the presence of cementite, whose hardness remains over 700 HV. Furthermore, a high quantity of chromium carbides precipitates at the weld bead due to the high carbon content of that zone associated with a high dilution. These changes cause an additional loss of strength, although part of the lost ductility is recovered.

− The breakage of the tensile test pieces took place preferably at the hardest zone: the interface for the preheated coupons and at the weld bead for the annealed coupons.

− Corrosion was lower for the annealed welds, although the presence of chromium carbide precipitates increases the corrosion susceptibility of the weld bead.

REFERENCES

Akdogan, G., Stolarski, T.A. (2003). Wear in metal/silicon nitride sliding pairs. *Ceram. Int.* 29 (4), 435–446. https://doi.org/10.1016/S0272-8842(02)00156-6.

Bedolla-Jacuinde, A., Arias, L., Hernández, B. (2003). Kinetics of secondary carbides precipitation in a high-chromium white iron. *J. Mater. Eng. Perform.* 12 (4), 371–382. https://doi.org/10.1361/105994903770342881.

Čanžar, P., Tonković, Z., Kodvanj, J. (2012). Microstructure influence on fatigue behaviour of nodular cast iron. *Mater. Sci. Eng. A* 556, 88–99. https://doi.org/10.1016/j.msea.2012.06.062.

Cárcel-Carrasco, F.-J., Pérez-Puig, M.-A., Pascual-Guillamón, M., Pascual-Martínez, R. (2016). An Analysis of the Weldability of Ductile Cast Iron Using Inconel 625 for the Root Weld and Electrodes Coated in 97.6% Nickel for the Filler Welds. *Metals* 6 (11), 283. https://doi.org/10.3390/met6110283.

Chamim, M., Triyono, Diharjo, K. (2017). Effect of electrode and weld current on the physical and mechanical properties of cast iron welding. *AIP Conference Proceedings* 1788, 030031. https://doi.org/10.1063/1.4968284.

El-Banna, E.M. (1999). Effect of preheat on welding of ductile cast iron. *Mater. Lett.* 41 (1), 20–26. https://doi.org/10.1016/S0167-577X(99)00098-1.

Gadhikar, A.A., Sharma, C.P., Goel, D.B., Sharma, A. (2011). Effect of heat treatment on carbides in 23-8-N steel. *Met. Sci. Heat Treat.* 53 (5–6), 293–298. https://doi.org/10.1007/s11041-011-9385-z.

Makar, J. (2000). A preliminary analysis of failures in grey cast iron water pipes. *Eng. Fail. Anal.* 7 (1), 43–53. https://doi.org/10.1016/S1350-6307(99)00005-9.

Moustafa, I., Moustafa, M., Nofal, A. (2000). Carbide formation mechanism during solidification and annealing of 17% Cr-ferritic steel. *Mater. Lett.* 42 (6), 371–379. https://doi.org/10.1016/S0167-577X(99)00213-X.

Pouranvari, M. (2010). On the weldability of grey cast iron using nickel based filler metal. *Mater. Des.* 31 (7), 3253–3258. https://doi.org/10.1016/j.matdes.2010.02.034.

Soffritti, C., Cazolari, L., Chicca, M., Bassi, R., Neri, A., Bazzocchi, L., Garagnani, G.L. (2020). Cast iron street furniture: A historical review. *Endeavour* 44 (3), 100721. https://doi.org/10.1016/j.endeavour.2020.100721.

Suárez-Sanabria, A., Fernández-Carrasquilla, J. (2006). Microstructure and mechanical properties of as-cast ferritic spheroidal cast iron for heavy section. *Rev. Metal.* 42 (1), 18-31. https://doi.org/10.3989/revmetalm.2006.v42.i1.3.

Vander Voort, G. (2005). *Microstructure of Ferrous Alloys. In Analytical Characterization of Aluminum, Steel, and Superalloys.* CRC Press, pp. 157–234.

You, Z., Lai, Y., Zeng, H., Yang, Y. (2020). Influence of water and sodium chloride content on corrosion behavior of cast iron in silty clay. *Constr. Build. Mater.* 238, 117762. https://doi.org/10.1016/j.conbuildmat.2019.117762.

Zhou, Y., Lu, Z., Zhan, M. (2007). An investigation of the erosion–corrosion characteristics of ductile cast iron. *Mater. Des.* 28 (1), 260–265. https://doi.org/10.1016/j.matdes.2005.07.011.